

The dynamic and thermodynamic processes dominating the reduction of global land monsoon precipitation driven by anthropogenic aerosols emission

Article

Accepted Version

Zhou, T., Zhang, W., Zhang, L., Zhang, X., Qian, Y., Peng, D., Ma, S. and Dong, B. ORCID: <https://orcid.org/0000-0003-0809-7911> (2020) The dynamic and thermodynamic processes dominating the reduction of global land monsoon precipitation driven by anthropogenic aerosols emission. *Science China Earth Sciences*, 63 (7). pp. 919-933. ISSN 1869-1897 doi: [10.1007/s11430-019-9613-9](https://doi.org/10.1007/s11430-019-9613-9) Available at <https://centaur.reading.ac.uk/90745/>

It is advisable to refer to the publisher's version if you intend to cite from the work. See [Guidance on citing](#).

To link to this article DOI: <http://dx.doi.org/10.1007/s11430-019-9613-9>

Publisher: Science China

the [End User Agreement](#).

www.reading.ac.uk/centaur

CentAUR

Central Archive at the University of Reading

Reading's research outputs online

The dynamic and thermodynamic processes dominating the reduction of global land monsoon precipitation driven by anthropogenic aerosols emission

**Tianjun ZHOU^{1,2,3*}, Wenxia ZHANG^{1,3}, Lixia ZHANG^{1,2}, Xuebin ZHANG⁴, Yun QIAN⁵,
Dongdong PENG^{6,1}, Shuangmei MA^{1,3}, Buwen DONG⁷**

¹State Key Laboratory of Numerical Modeling for Atmospheric Sciences and Geophysical Fluid Dynamics, Institute of Atmospheric Physics, Chinese Academy of Sciences, Beijing 100029, China.

² CAS Center for Excellence in Tibetan Plateau Earth Sciences, Chinese Academy of Sciences (CAS), Beijing 100101, China.

³University of Chinese Academy of Sciences, Beijing 100049, China.

⁴Environment and Climate Change Canada, 4905 Dufferin Street, Toronto, ON, Canada.

⁵Atmospheric Science and Global Change Division, Pacific Northwest National Laboratory, Richland, Washington 99352, USA.

⁶Institute of Tropical and Marine Meteorology, China Meteorological Administration, Guangzhou 510640, China

⁷National Centre for Atmospheric Science, Department of Meteorology, University of Reading, Reading RG6 6BB, UK.

*Corresponding author (email: zhoutj@lasg.iap.ac.cn)

22 **Abstract**

23 Changes in monsoon precipitation have profound social and economic impacts as more than two-
24 thirds of the world's population lives in monsoon regions. Observations show a significant
25 reduction in global land monsoon precipitation during the second half of the 20th century.
26 Understanding the cause of this change, especially possible anthropogenic origins, is important.
27 Here, we compare observed changes in global land monsoon precipitation during 1948~2005 with
28 those simulated by 5 global climate models participating in the Coupled Model Inter-comparison
29 Project-phase 5 (CMIP5) under different external forcings. We show that the observed drying trend
30 is consistent with the model simulated response to anthropogenic forcing and to anthropogenic
31 aerosol forcing in particular. We apply the optimal fingerprinting method to quantify
32 anthropogenic influences on precipitation and find that anthropogenic aerosols may have
33 contributed to 102% (62~144% for the 5~95% confidence interval) of the observed decrease in
34 global land monsoon precipitation. A moisture budget analysis indicates that the reduction in
35 precipitation results from reduced vertical moisture advection in response to aerosol forcing. Since
36 much of the monsoon regions, such as India and China, have been experiencing rapid
37 developments with increasing aerosol emissions in the past decades, our results imply a further
38 reduction in monsoon precipitation in these regions in the future if effective mitigations to reduce
39 aerosol emissions are not deployed. The observed decline of aerosol emission in China since 2006
40 helps to alleviate the reducing trend of monsoon precipitation.

41 **Key words:** global monsoon, detection, attribution, aerosol forcing

44 **1 Introduction**

45 Changes in monsoon precipitation are of great scientific importance and significant societal
 46 concern owing to the facts that monsoon affects a large population. The global monsoon system
 47 includes Asian-Australia monsoon (South Asian, East Asian, Northwestern Pacific and Australian
 48 monsoons), African monsoon (North African and South African monsoons) and American
 49 monsoon (North American and South American monsoons). A number of observational studies
 50 have reported a significant drying trend in the global monsoon precipitation during the second half
 51 of the 20th century (Wang and Ding, 2006; Zhou et al., 2008a; Zhang and Zhou, 2011; Polson et
 52 al., 2014). Understanding the causes of these changes is vital to infrastructural planning, water
 53 resource management, and sustainable development.

54 The changes of global monsoon are modulated by several factors. Different factors including
 55 the greenhouse gases (GHGs) (Kitoh et al., 2013; Song et al., 2014; Chen and Zhou, 2015),
 56 anthropogenic aerosols (AAs) (Held et al., 2005; Lau et al., 2006; Meehl et al., 2008; Bollasina et
 57 al., 2011; Qian et al., 2011; Jiang et al., 2013, 2015; Guo et al., 2013; Wu et al., 2013; Polson et
 58 al., 2014; Song et al., 2014; Li et al., 2016; Zhang et al., 2018), and natural internal variability of
 59 the climate system, such as the Inter-decadal Pacific Oscillation (IPO) (Zhu and Yang, 2003; Yang
 60 et al., 2004; Zhou et al., 2008b; Li et al., 2010; Wang et al., 2012; Huang et al., 2020), have been
 61 proposed to explain the observed reduction in monsoon precipitation. The impact of individual
 62 factors is regional dependent, including the sign and magnitude of impact (Polson et al., 2014;
 63 Pascale et al., 2017).

64 Greenhouse gases can modulate monsoon circulations in two ways. On the one hand, the
 65 greenhouse gases can intensify the land-sea thermal contrast and the hemispheric thermal contrast
 66 to enhance East Asian summer monsoon. On the other hand, it would broaden the descent branch
 67 of Hadley circulation and weaken Walker circulation by increasing the atmospheric stability,
 68 weakening the monsoon circulation. Competition between the two mechanisms leads to a slightly
 69 increase in East Asian summer monsoon (Song et al., 2014; Lau and Kim, 2017). Greenhouse
 70 gases may also result in uneven warming of sea surface temperature, thus modulating regional
 71 monsoon circulations. In the late half of 20th century, the warming in the tropical Northwestern
 72 Pacific has led to anomalous circulation anomalies at lower level and transported more dry air to
 73 South Asia, resulting in reduced rainfall over South Asia (Annamalai et al., 2013).

74 The impact of anthropogenic aerosol forcing is more complex. Although the impact of
 75 anthropogenic aerosols on the decline of northern hemispheric monsoon precipitation in the past
 76 decades has been detected (Polson et al., 2014), there is no consensus on the dominant dynamical
 77 processes. In the East Asian summer monsoon season, aerosols could reduce the land-sea thermal
 78 contrast and increase atmospheric stability, thus weakening the summer monsoon circulation
 79 (Song et al., 2014). In South Asia, aerosols could reduce the incoming shortwave radiation, cool the
 80 surface, reduce local evaporation and water vapor content. It could also increase the atmospheric
 81 stability and reduce the hemispheric thermal contrast, resulting in a weaker South Asian summer
 82 monsoon and less precipitation (Lau et al., 2006; Bollasina et al., 2011; Salzmann et al., 2014; Guo
 83 et al., 2013). In addition, different types of aerosols exert different impacts (e.g., the local and
 84 remote forcing of aerosols) on regional monsoons (Jiang et al., 2013; Dong et al., 2016; Wang et
 85 al., 2017). Recent studies documented that the land use and land cover changes in the recent
 86 decades can alter the albedo and evaporation to reduce monsoon precipitation (Krishnan et al.,
 87 2016; Paul et al., 2016).

88 In addition to the external forcings, the monsoon system is influenced by internal variability
89 of the climate. On the decadal to inter-decadal time scales, the Atlantic Multi-decadal Oscillation
90 (AMO) and Pacific Decadal Oscillation (PDO/IPO) can exert impacts on regional to hemispheric
91 monsoon precipitation changes through modulating the Walker and Hadley circulation (Zhou et
92 al., 2008b; Li et al., 2010; Krishnamurthy and Krishnamurthy, 2014; Wang et al., 2013; Jiang and
93 Zhou, 2019). Thus, the changes in the global monsoon system are the compound results of external
94 forcings and internal variability. Due to the complexity of the global monsoon system, it is still
95 unclear about the main cause and mechanisms behind the declined precipitation in global land
96 monsoon since the 1950s.

97 Here, we consider these multiple factors in a unified framework to determine the dominant
98 factor, quantify its contribution, and physically understand how competing factors influence the
99 observed changes from a global perspective. To understand the potential relative contributions of
100 natural (solar variations and volcanoes) and anthropogenic (well-mixed GHGs, aerosols) forcings
101 to the drying trend in global land monsoon domains, ensemble simulations from 5 state-of-the-art
102 coupled climate system models are used to attribute the observed long-term trend. The rigorous
103 “optimal fingerprinting” method is used to examine whether the anthropogenic influence is
104 detectable and attributable in the historical changes of global land monsoon precipitation. A
105 moisture budget analysis is then performed to understand the physical processes that dominate the
106 detected historical changes. We show evidences that the drying trend in monsoon precipitation
107 results from the reduction in vertical moisture advection due to aerosol forcing, the underlying
108 physical processes include a thermodynamic effect due to the reduction in atmospheric humidity
109 and a dynamic effect due to weakening of the land-sea thermal contrast and thus monsoon
110 circulation.

111 The remainder of the paper is organized as following. The data and methods are described
112 in section 2. The analysis results are presented in section 3. Section 4 summarizes the major
113 findings along with a discussion.

114 **2 Data and Methods**

115 **2.1 Data**

116 Multiple observational datasets are compared to better account for uncertainties in the
117 observations. The six observational monthly precipitation datasets used in our analysis include
118 Climate Research Unit TS V4.01 (CRU) (Harris et al., 2014), Global Precipitation Climatology
119 Center Full V6 (GPCC) (Schneider et al., 2014), University of Delaware precipitation V4.01
120 (Delaware) (Willmott et al., 2001), NOAA’s Precipitation Reconstruction over Land (PREC/L)
121 (Chen et al., 2002), Variability Analysis of Surface Climate Observations (VASClimO, V1.1) from
122 1950~2005 (Beck et al., 2005); and GHCN V2 (Peterson et al., 1997). All data sets are regridded
123 to a common $2.5^\circ \times 2.5^\circ$ resolution. We focus on the common time period of 1948~2005. An
124 ensemble average of CRU, GPCC, Delaware, PREC/L and GHCN data is used in our analysis.
125 The precipitation dataset from VASClimO is not employed when calculating the ensemble mean
126 due to a shorter time coverage, we note that it also shows a similar trend over the common time
127 period of 1951~2000 (Fig. 1).

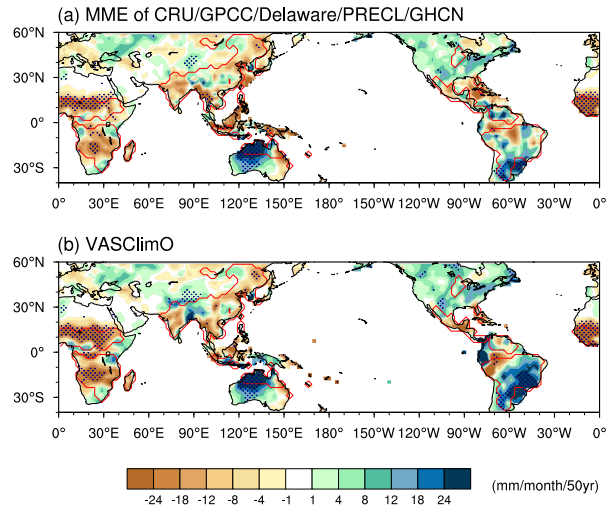


Figure 1. The spatial distributions of the linear trends in the local summer precipitation during 1951~2000 derived from (a) the multi-observation ensemble mean of CRU, GPCC, University of Delaware, PREC/L, and GHCN, and (b) VASClimo. Stippling indicates the 5% significance level. Red lines denote the global land monsoon regions.

We analyze 5 CMIP5 models (i.e., CanESM2, CSIRO-Mk3-6-0, GFDL-CM3, GISS-E2-H, and GISS-E2-R), which provide separate forcing simulations under greenhouse gases, anthropogenic aerosols, and natural forcing (NAT) forcings only, meanwhile each individual forcing simulation includes multiple realizations (Table 1; Taylor et al., 2012). The 5 models provide a total of 101 simulations, including 32 historical, 23 historical GHG, 23 historical anthropogenic aerosols, and 23 historical natural experiments. The historical simulations (*ALL-forcing*) are forced by both natural forcings (i.e., solar variability and volcanic aerosols) and anthropogenic forcings (i.e., GHGs and anthropogenic aerosols) (Table 2). The historical GHG (*GHG-forcing*), the historical anthropogenic aerosol (*AA-forcing*), and the historical natural (*NAT-forcing*) simulations are the same as the historical simulations, except that they are only forced by well-mixed GHGs, aerosols, or natural forcings, respectively. All model data are regressed onto a common $2.5^\circ \times 2.5^\circ$ grid with bilinear interpolation. The global land monsoon areas (see definitions below) in the models are masked by the observations.

Table 1. Details of the 5 CMIP5 Models used in this study. All five models include a representation of the direct and indirect aerosol effects.

Model	CanESM2	CSIRO-Mk3-6-0	GFDL-CM3	GISS-E2-H	GISS-E2-R
Institute	CCCma Canada	CSIRO-QCCCE Australia	NOAA-GFDL USA	NASA-GISS USA	NASA-GISS USA
Horizontal resolution	64*128	96*192	90*144	90*144	90*144
ALL	5	10	5	6	6
Ensemble size					
GHG	5	5	3	5	5

	AA	5	5	3	5	5
	Nat	5	5	3	5	5
Natural forcing agents	Solar	SOLARIS	SOLARIS	SOLARIS	SOLARIS	SOLARIS
	Volcanic	S	S	S	S	S
Anthropogenic forcing agents	GHG	IIASA	IIASA	IIASA	IIASA	IIASA
	Aerosol	E1	E2	E1	C	C

151
152 SOLARIS: <http://sparcsolaris.gfz-potsdam.de/cmip5.php>;
153 S: Sato et al. (1993);
154 C: The three-dimensional aerosol distributions specified as the monthly 10-year mean aerosol concentrations,
155 derived using the CAM-Chem model, which is driven by the Lamarque et al. (2010); the anthropogenic aerosols
156 include organic carbon (OC), black carbon (BC) and sulfur dioxide (SO₂).
157 E1: the anthropogenic aerosol emissions taken from the Lamarque et al. (2010);
158 E2: Same as E1 but with the black carbon increased uniformly by 25% and the organic aerosol increased by 50%
159 (Rotstayn et al. 2012).
160

161 **Table 2.** The list of the CMIP5 control simulations used for evaluating the internal climate
162 variability. The overall drift of the control simulation is removed by subtracting a linear trend over
163 the full period.

No.	Model	Length (year)	Number of non-overlapping 58-year segments non-overlapping 58-year segments
1	bcc-csm1-1	500	8
2	BNU-ESM	559	9
3	CCSM4	501	8
4	CNRM-CM5	600	10
5	CSIRO-Mk3-6-0	500	8
6	CanESM2	996	17
7	FGOALS-g2	900	15
8	GFDL-CM3	500	8
9	GISS-E2-H	480	8
10	GISS-E2-R	850	14
11	HadGEM2-ES	336	5
12	IPSL-CM5A-LR	1000	17
13	MIROC-ESM	531	9

14	MIROC-ESM-CHEM	255	4
15	MRI-CGCM3	500	8
16	NorESM1-M	501	8
17	ACCESS1-0	250	4
18	CESM1-CAM5	319	5
19	FGOALS-s2	501	8
20	HadGEM2-CC	240	4
21	MIROC5	670	11
22	MPI-ESM-LR	1000	17

164

165

166

2.2 Definition of global monsoon region

167 Global monsoon region is defined as the region with the annual range of precipitation (local
 168 summer minus local winter) greater than 2.0 mm day^{-1} and local summer precipitation exceeding
 169 55% of the annual total amount (Wang and Ding., 2008). In the northern (southern) hemisphere,
 170 summer (winter) is from May to September, and winter (summer) is from November to March.

171

2.3 Detection and attribution

172 According to the IPCC Assessment report, “*Detection of change is defined as the process of*
 173 *demonstrating that climate or a system affected by climate has changed in some defined statistical*
 174 *sense without providing a reason for that change. An identified change is detected in observations*
 175 *if its likelihood of occurrence by chance due to internal variability alone is determined to be small.*
 176 *Attribution is defined as the process of evaluating the relative contributions of multiple causal*
 177 *factors to a change or event with an assignment of statistical confidence.*” (Hegerl et al., 2010;
 178 Bindoff et al., 2013; Sun et al., 2013). In the optimal fingerprinting method, observed summer
 179 precipitation anomalies averaged over the global land monsoon regions were multi-linearly
 180 regressed against the model-based signals via a generalized total least square (TLS) method (Allen
 181 and Stott, 2003).

$$182 \quad y = \sum_{i=1}^m \beta_i (x_i - \varepsilon_{x_i}) + \varepsilon_0 \quad (1)$$

183 where y represents the observation, x_i represents the climate response to the i th external
 184 forcing considered (i.e., the fingerprint or signal of the specific external forcing (e.g., ALL-forcing,
 185 GHG-forcing, AA-forcing, or NAT-forcing)). The time series is calculated with five-year non-
 186 overlapping averages for the global land monsoon region as a whole. ε_{x_i} represents the effect of
 187 internal variability in the estimated responses due to limited number of available simulations. m
 188 represents the size of the external forcings. ε_0 represents the noise in the observation and is
 189 associated with internal climate variability. β_i is the scaling factor.

190 Detection of a specific response is claimed if the corresponding scaling factor is significantly
 191 inconsistent with zero (i.e., the lower bound of 90% confidence interval of a scaling factor is larger
 192 than zero). Furthermore, attribution is claimed if the scaling factor is inconsistent with zero and
 193 consistent with one (i.e., the 90% confidence interval includes one), meanwhile other plausible

194 causes are excluded (Hegerl et al., 2010). The ensemble simulations underestimate (overestimate)
195 the observed response with a β greater (less) than one.

196 The attributable changes from different external forcings can be further estimated based on the
197 derived scaling factors (e.g., Allen and Stott, 2003; Sun et al., 2014; Xu et al., 2015). For each
198 external forcing, it is estimated as the linear least-square trend from the ensemble mean simulations
199 multiplied by the corresponding scaling factor. The uncertainty ranges of the attributable changes
200 are estimated based on the 90% confidence intervals of β , which involve the effects of internal
201 variability in both observations and simulations.

202 To estimate the internal variability (i.e., noise), a total of 12489 years in the pi-Control
203 simulations from the 22 CMIP5 models were divided into non-overlapping 58-year chunks, which
204 provided 204 chunks (Table 2). In addition, the intra-ensemble variability (i.e., the residuals of the
205 historical simulations after subtracting their respective ensemble means) was provided for a total
206 of 101 runs (Table 1). For each historical simulation, the period 1890-2005 was used, which
207 provided 2 chunks of the 58-year segments. Thus, 202 chunks of noise estimation were derived
208 from the intra-ensemble variability. In total, the 406 chunks of noise estimation were divided into
209 two independent sets, where one set was used for optimization and the other was used for the
210 residual consistency test (Allen and Tett, 1999; Zhang et al., 2007; Xu et al., 2015).

211 We conduct the one-signal detection analysis for local summer precipitation changes averaged
212 over the global land monsoon region. The optimal detection is performed in a reduced space
213 spanned by leading empirical orthogonal functions (EOFs) for the model-simulated internal
214 variability (e.g., Zhang et al., 2007; Sun et al., 2014; Xu et al., 2015). The number of EOFs retained
215 is based on the residual consistency test (Allen and Tett, 1999; Allen and Stott, 2003). To test the
216 robustness of the detection results, we perform the detection analysis using a range of numbers of
217 EOFs retained.

218 **2.4 Moisture budget analysis**

219 Within the atmosphere, precipitation is balanced by the sum of evaporation, convergence of the
220 column-integrated moisture flux, and the residual (which mainly includes transient eddies and
221 contributions from surface processes due to topography) (Chou et al., 2013a):

$$222 P = E - \langle \nabla \cdot \mathbf{V}q \rangle + \delta \quad (2)$$

223 where P represents precipitation, E represents evaporation, \mathbf{V} is the wind vector, q
224 represents the specific humidity, and $-\langle \nabla \cdot \mathbf{V}q \rangle$ represents the convergence of the column-
225 integrated moisture flux. The term $-\langle \nabla \cdot \mathbf{V}q \rangle$ can be divided into two terms: vertical moisture
226 advection ($-\langle \omega \partial_p q \rangle$) and horizontal moisture advection ($-\langle \mathbf{V}_h \cdot \nabla_h q \rangle$). Then, the changes in
227 precipitation can be expressed by changes in evaporation, horizontal moisture advection, vertical
228 moisture advection, and residuals, as in Eq. (3).

$$229 P' = E' - \langle \omega \partial_p q' \rangle - \langle \mathbf{V}_h \cdot \nabla_h q' \rangle + \delta' \quad (3)$$

230 where prime indicates departure from the climatology. The subscripts p and h denote the
231 pressure and the horizontal direction, respectively. \mathbf{V}_h represents the horizontal wind vector, and
232 ∇_h is the horizontal differential operator. The vertical moisture advection change, $-\langle \omega \partial_p q' \rangle$ is
233 further approximated as the sum of the thermodynamic contribution, $-\langle \bar{\omega} \partial_p q' \rangle$, the dynamic
234 contribution, $-\langle \omega' \partial_p \bar{q} \rangle$, and the nonlinear term, $-\langle \omega' \partial_p q' \rangle$. The overbar denotes the
235 climatology. $-\langle \bar{\omega} \partial_p q' \rangle$ is associated with changes in water vapor, which are mainly induced by

temperature changes; $-\langle \omega' \partial_p \bar{q} \rangle$ is associated with changes in pressure velocity, which are mainly induced by atmospheric circulation changes; $-\langle \omega' \partial_p q' \rangle$ involves changes in both vertical circulation and moisture and is found to be relatively small. Hence, Eq. (3) can be approximated by:

$$P' \approx E' - \langle \bar{\omega} \partial_p q' \rangle - \langle \omega' \partial_p \bar{q} \rangle - \langle \mathbf{V}_h \cdot \nabla_h q' \rangle \quad (4)$$

Changes in precipitation and evaporation are coupled with each other; thus the causal relationship cannot be distinguished by the moisture budget analysis.

3 Results

3.1 Comparison between observations and model simulations

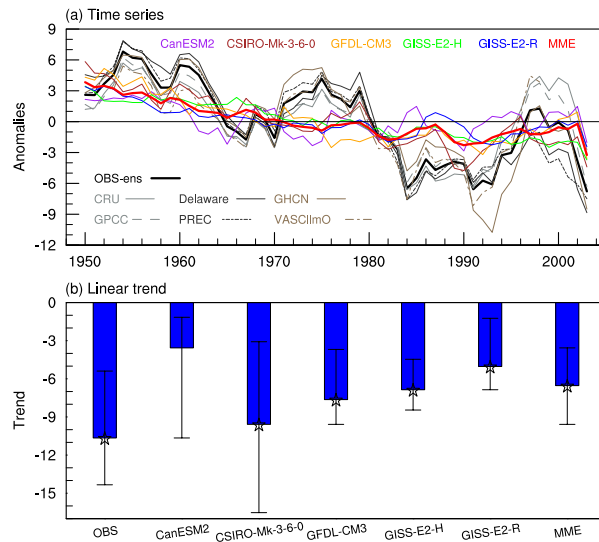
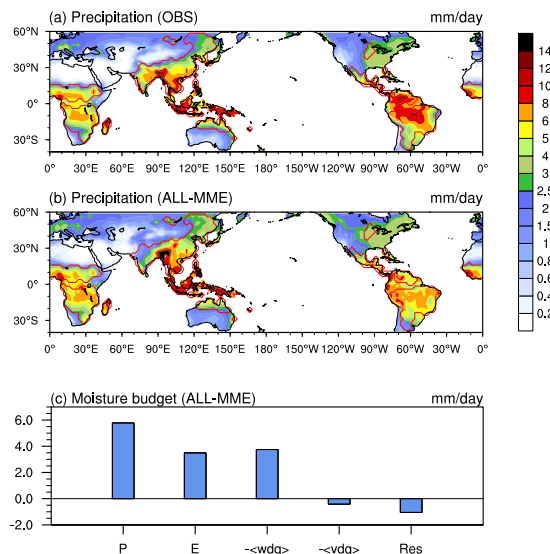


Figure 2. Changes in global land monsoon precipitation during 1948~2005. (a) Time series of local summer precipitation during 1948~2005 averaged over the global land monsoon regions derived from multiple observations and ALL-forcing simulations from the 5 CMIP5 models. Precipitation anomalies (units: mm month^{-1}) are with respect to 1948~2005 and smoothed with a 5-year running mean. The thick black line denotes the multi-observation ensemble mean (without VASClmo due to its shorter time coverage of 1951~2000), and the thick red line denotes the multimodel ensemble mean (MME) of the historical simulations. (b) Linear trends ($\text{mm month}^{-1} (58\text{yr})^{-1}$) in local summer precipitation averaged over the global land monsoon regions. Bars represent the ensemble-mean trends, and the error lines show the range of different realizations. Trends that are statistically significant at the 5% level are marked with stars.

We used five sets of observational precipitation data to identify the trends during 1948~2005 in the global land monsoon domain (Fig. 2a). The ensemble mean of the 5 datasets shows a remarkable reduction in monsoon precipitation during the period 1948~2005 (Fig. 2a), with a linear trend of -10.55 (ranging from -5.39 to -14.34) $\text{mm month}^{-1} (58\text{yr})^{-1}$, which corresponds to -5.92% (-3.02% to -8.22%) of the 1961~1990 climatology and is statistically significant at the 1% level (Fig. 2b). The decreasing trend is consistent with previous studies that used more or less data (Wang and Ding, 2006; Zhou et al., 2008a, b; Zhang and Zhou, 2011), demonstrating the robustness of the drying trend.

265
266
267
268
269
270
271
272

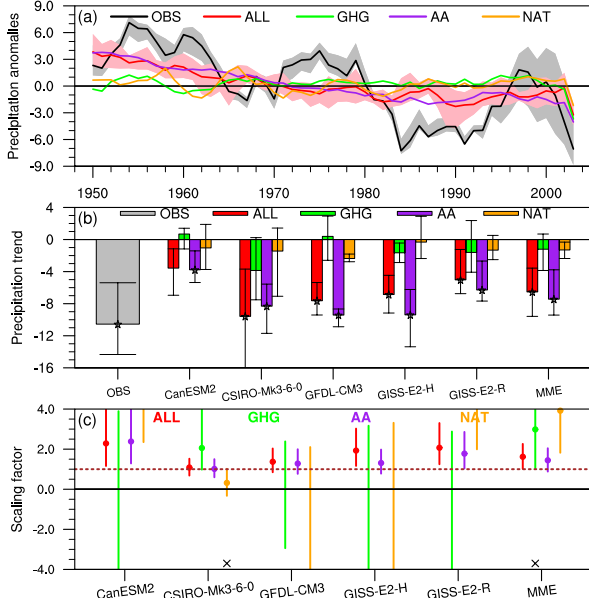
To estimate the contributions of external forcings, we compare the observed changes to those simulated by the 5 state-of-the-art coupled climate system models of the CMIP5. The 5 models reasonably reproduce the climatology of local summer precipitation over the global land monsoon regions, with a pattern correlation coefficient of 0.84 between the multi-observation ensemble mean and the multimodel ensemble mean (MME), calculated on a common $2.5^\circ \times 2.5^\circ$ spatial resolution (only land monsoon regions are retained), forming a solid basis for our analysis of the long term monsoon precipitation changes (Fig. 3a and b).



273
274 **Figure 3.** The climatology (units: mm day^{-1}) of the global land summer precipitation in (a) the
275 observations and (b) the MME of the ALL-forcing historical simulations. The red lines denote
276 the global land monsoon region. (c) The climatological moisture budget terms averaged over the
277 global land monsoon region in the MME of the ALL-forcing simulations. P-E is precipitation
278 minus evaporation, $-\langle wdq \rangle$ is the vertical moisture advection, $-\langle vdq \rangle$ is the horizontal
279 moisture advection, and Res is the residual term.

280
281
282
283
284
285
286
287
288

In terms of the trends in the local summer precipitation, the all-forcing ensemble (ALL) reasonably captures the drying trend over the global land monsoon domain (Fig. 2a). The drying trend in the MME is $-6.49 \text{ mm month}^{(-1)} (58 \text{ years})^{(-1)}$, or -3.89% of the 1961~1990 climatology, which is within the range of multiple observations (Fig. 2b). All the 5 models are qualitatively consistent in reproducing the drying trend, although with differences in magnitudes. The consistent changes in the local summer global land monsoon precipitation between the observations and the ALL-forcing historical simulations imply that external forcing has played a role in driving the long term changes in the local summer precipitation.



289
290
291
292
293
294
295
296
297
298
299
300
301
302
303

Figure 4. Detection and attribution of global land monsoon precipitation changes under different forcing agents. (a) Time series of the 5-year running average global land monsoon precipitation anomalies with respect to the 1948~2005 mean (units: mm month^{-1}) in the multi-observation ensemble mean and the multimodel ensemble mean under individual forcings. Gray shadings represent the range of different observations, and light pink shadings represent the range of ALL-forcing simulation results. (b) Linear trends (units: $\text{mm month}^{-1} 58\text{yr}^{-1}$) in global land monsoon precipitation. Bars represent the ensemble mean, which are labeled with stars if the trend is statistically significant at the 5% level. Error lines represent the ranges of different realizations. (c) The results of the optimal fingerprinting detection at an EOF truncation of 10. Solid circles and error bars represent the best estimate and the 5–95% uncertainty range of the scaling factors, respectively. The cross symbols indicate failure of the residual consistency test at the 10% level. In (a)–(c), red represents ALL-forcing, green represents GHG-forcing, purple represents AA-forcing and orange represents NAT-forcing.

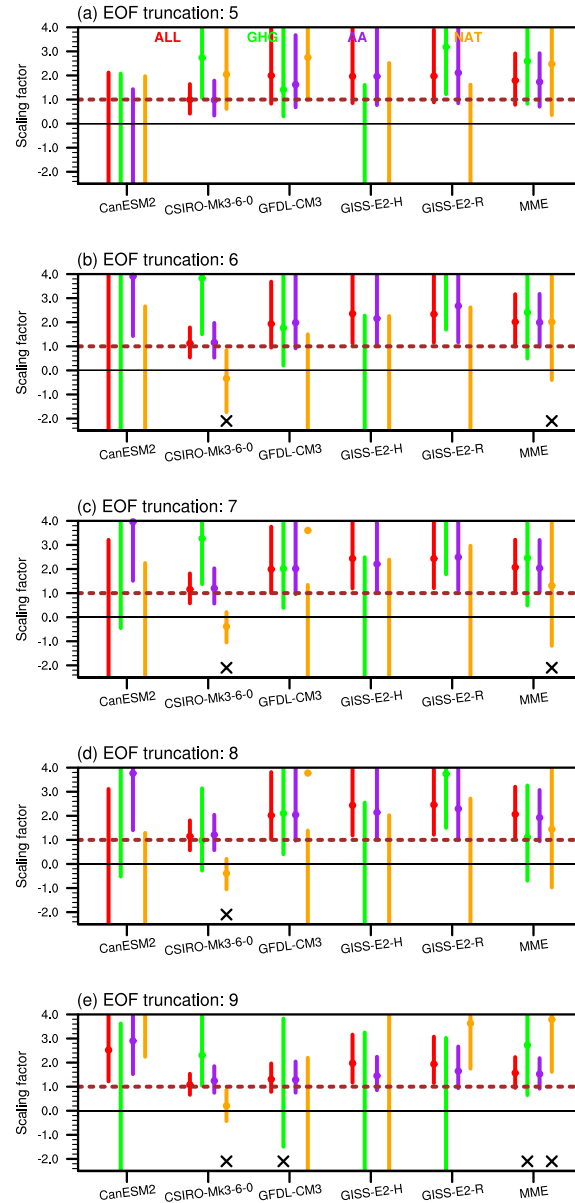
304
305
306
307
308
309
310
311
312
313
314
315
316
317
318
319

A further comparison of the individual ensembles forced with different forcing combinations reveals that the significant drying trend over the global land monsoon regions originates from anthropogenic influences mainly caused by aerosols (Fig. 4a and b). The dominance of the aerosol forcing on the drying trend is evident in all the 5 models (Fig. 4b). In contrast, the trends of both the GHGs and natural forcing ensembles are weak and statistically insignificant (Fig. 4a and b).

3.2 Detection and attribution of the anthropogenic forcing

The temporal evolutions of the observed and simulated precipitation are compared quantitatively using the “optimal fingerprint” method, a regression procedure that has been widely used in the community of detection studies. We focus on the ensembles of the 5 models. Over the global land monsoon regions, the scaling factors for the ALL-forcing and AA-forcing simulations are significantly greater than zero, indicating that the ALL-forcing and the AA-forcing had a detectable influence on the decrease in global monsoon precipitation. The scaling factors for the ALL-forcing and AA-forcing simulations are consistent with unity, indicating that the decline in global land monsoon precipitation can be attributed to aerosol emissions (Fig. 4c). We note that the detected seasonal mean precipitation changes is different to that of extreme precipitation at regional scales. For example, while the increases in greenhouse gases has had a detectable

320 contribution to the observed shift toward heavy precipitation in the eastern China, the
 321 anthropogenic aerosols partially offset the effect of the greenhouse gases forcing, but cannot be
 322 detected by the optimal fingerprint method (Ma et al., 2017).



323
 324 **Figure 5.** The results of optimal fingerprinting detection at EOF truncations of 5~9. Solid circles
 325 and error bars are the best estimate and the 5~95% uncertainty range of scaling factors, respectively.
 326 Cross symbols indicate fail of the residual consistency test at the 10% level. The effects of ALL
 327 and AA are detectable over a wide range of EOF truncations ranging from 5~10.
 328

329 The detectable effects of the ALL and AA forcings are consistent in all individual models and
 330 over a wide range of EOF truncations ranging from 5~10, demonstrating the robustness of the
 331 detection results (Fig. 4c and Fig. 5). The effects of GHG and NAT forcings are not detected, either
 332 due to the failure of the residual consistency test or the scaling factor spanning zero, which vary
 333 substantially across individual models (Fig. 4c and Fig. 5).

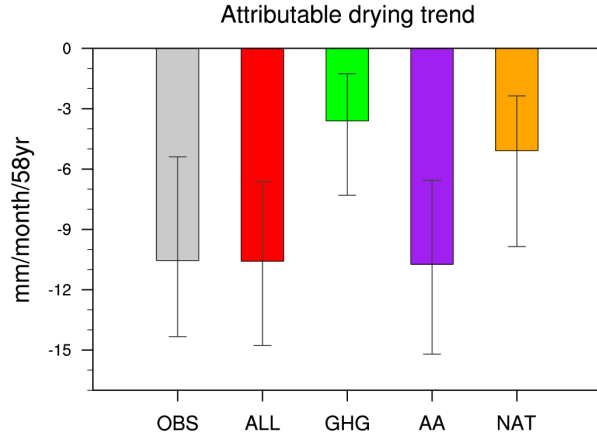
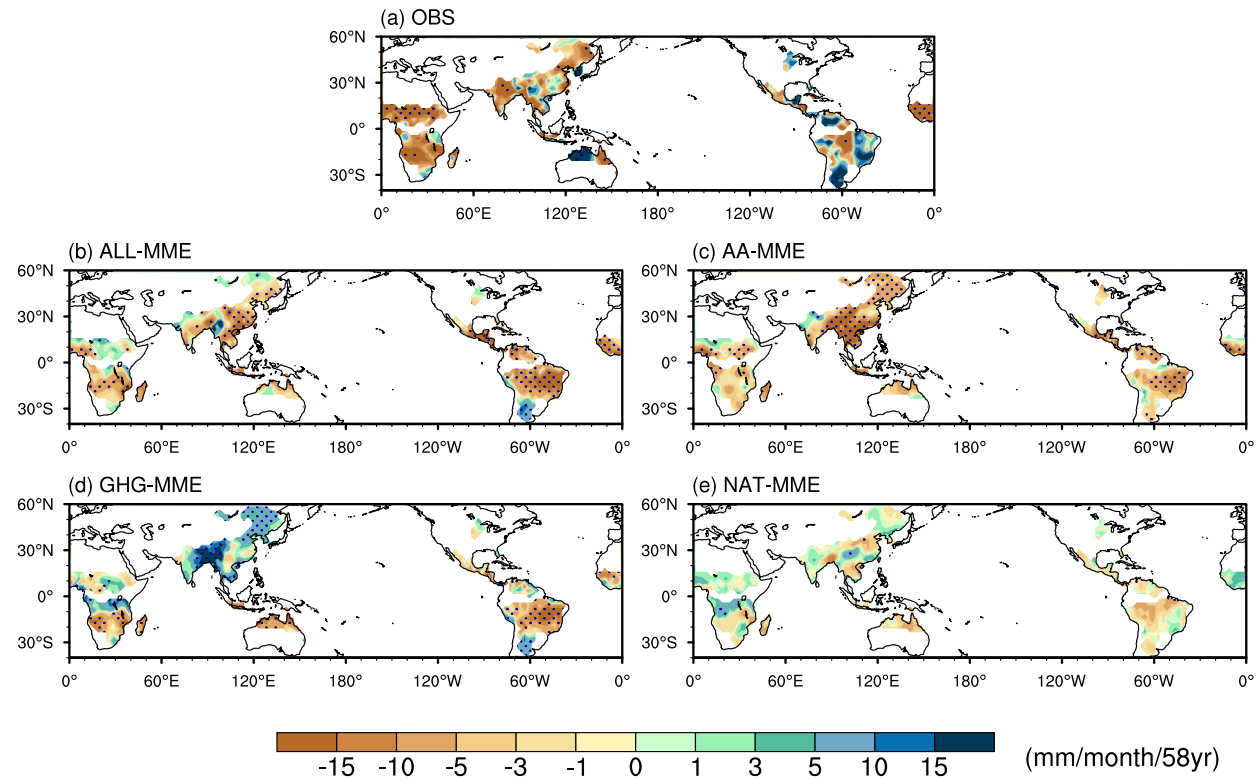


Figure 6. Best estimates of the attributable drying trends due to ALL, GHG, AA, and NAT forcings from the one-signal analysis, along with their 5~95% confidence intervals. For observations (gray bars), the ensemble mean and ranges of multi-observations are shown.

We further estimate the drying trends attributable to different forcing agents by multiplying the simulated linear trends in the MME with respective scaling factors from the one-signal detection analysis (Fig. 6). The ALL forcing has contributed to approximately 100% (63~140% for the 5~95% confidence interval) of the observed trend in the global land monsoon precipitation during 1948~2005 ($-10.55 \text{ mm month}^{-1} (58\text{yr})^{-1}$). In particular, the anthropogenic aerosols have contributed to 102% (62~144%) of the observed trend.

3.3 Physical processes of difference anthropogenic forcings on precipitation changes



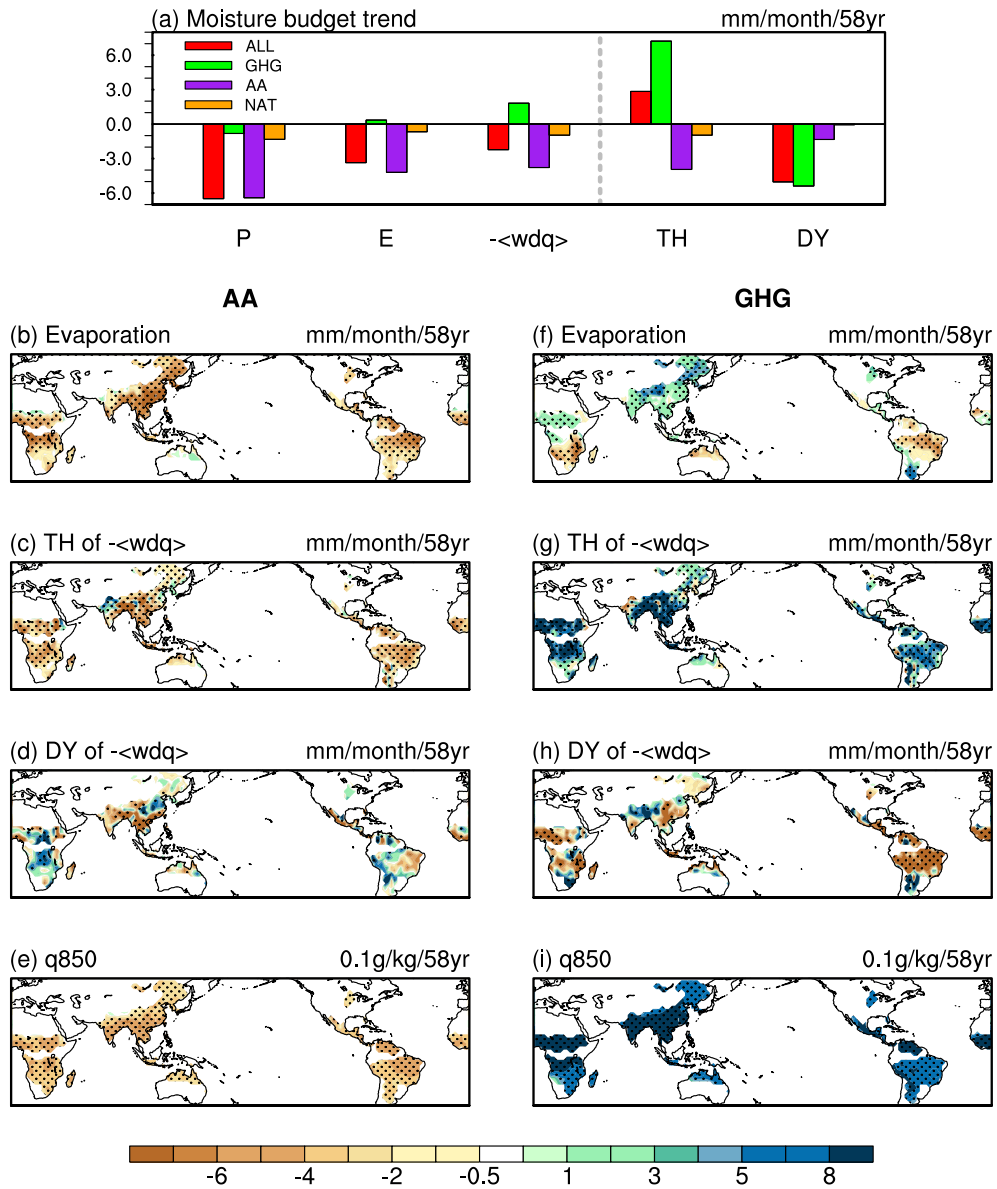
346

347 **Figure 7.** Spatial patterns of linear trends in local summer precipitation under different forcings.
348 The spatial distributions of linear trends in local summer precipitation during 1948~2005 derived
349 from the multi-observation ensemble mean (a), and the multimodel ensemble mean of ALL-
350 forcing simulations (b), AA-forcing simulations (c), GHG-forcing simulations (d), and NAT-
351 forcing simulations (e). Units are $\text{mm month}^{-1} (58\text{yr})^{-1}$. Stippling indicates the 5% significance
352 level. Only the global land monsoon regions are shown.

353
354 What are the regional features of the monsoon precipitation trends? In the observations, the
355 drying trends are significant in the North and South African monsoon regions, the South and East
356 Asian monsoon regions, part of the Australian monsoon region, and most parts of the North and
357 South American monsoon regions (Fig. 7a). The simulated (ALL-forcing run) large-scale drying
358 trend in precipitation over the global land monsoon regions is generally consistent with the
359 observed pattern, exhibiting more spatially coherent features (Fig. 7b). Regional discrepancies are
360 seen with drying overestimations in the eastern part of the South American monsoon region and
361 underestimations in the eastern part of the North African monsoon region.

362 Comparisons of the spatial patterns of the precipitation trend under individual forcings confirm
363 the dominant effect of aerosols on the drying trends in the South and East Asian monsoon regions,
364 the North and South American monsoon regions, and part of the African monsoon region (Fig. 7c).
365 The impact of the GHG forcing is more pronounced in the South and East Asian monsoon regions
366 and part of the African monsoon region, leading to wetter conditions (Fig. 7d) and, thus, partly
367 compensating the drying trends caused by aerosols (Fig. 7c). It is worth noting that the GHG
368 forcing has also led to drying conditions in the American monsoon regions (Fig. 7d), which is
369 consistent with simulations driven by an increase in CO_2 due to increased atmospheric stability
370 (Pascale et al., 2017). No significant trends are seen in the natural forcing ensembles (Fig. 7e).

371 How did the anthropogenic forcings affect the changes in the global land monsoon
372 precipitation? A moisture budget analysis is conducted over the global land monsoon regions
373 during 1948~2005. For the climate mean states, the global land monsoon precipitation is generally
374 balanced by evaporation and vertical moisture advection, whereas the contributions of the
375 horizontal moisture advection and residuals are relatively small and negligible (Fig. 3c).



376

377 **Figure 8.** Moisture budget analysis for the drying trend in precipitation. (a) The trends in moisture
 378 budget terms averaged over the global land monsoon region. The vertical moisture advection
 379 ($-\langle wdq \rangle$) is separated into a thermodynamic term (TH) and a dynamic term (DY). The red,
 380 green, purple and orange bars denote the MME of the ALL, GHG, AA, and NAT forcings,
 381 respectively. (b)-(i) Spatial patterns of linear trends in evaporation (b, f), the thermodynamic (c, g)
 382 and dynamic (d, h) terms of the vertical moisture advection, and the specific humidity at 850 hPa
 383 (e, i) during 1948~2005 in the multimodel mean of the AA-forcing (b-e) and GHG-forcing (f-i)
 384 simulations. Stippling indicates the 5% significance level. Units are $\text{mm month}^{-1} (58\text{yr})^{-1}$, except
 385 for figures (e) and (i), whose units are $0.1 \text{ kg}^{-1} (58\text{yr})^{-1}$.

386

387 For the linear trend during 1948~2005 in both the ALL-forcing and AA-forcing experiments,
 388 the drying trend in precipitation over the global land monsoon regions is dominated by the vertical

moisture advection, which is further separated into a thermodynamic and dynamic component (Fig. 8a). The thermodynamic increase in moisture advection (higher humidity due to higher temperature) in response to GHG forcing is largely offset by the decrease in the dynamic component (enhanced atmospheric stability and weakening of tropical circulation (Held et al., 2006; Schneider et al., 2010; Chou et al., 2013a, b)). Therefore, the net effect of moisture advection change is weak due to GHG forcing. Both the thermodynamic and dynamic effects of AA cause a reduction in the vertical moisture advection, where the thermodynamic effect is dominant (Fig. 8a).

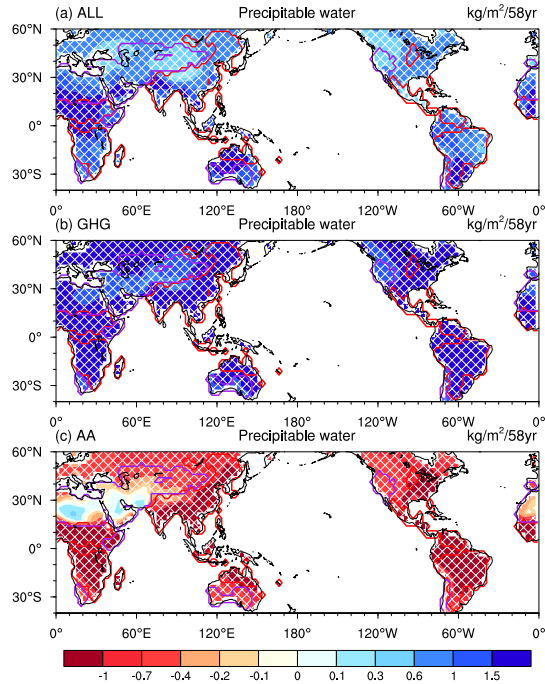
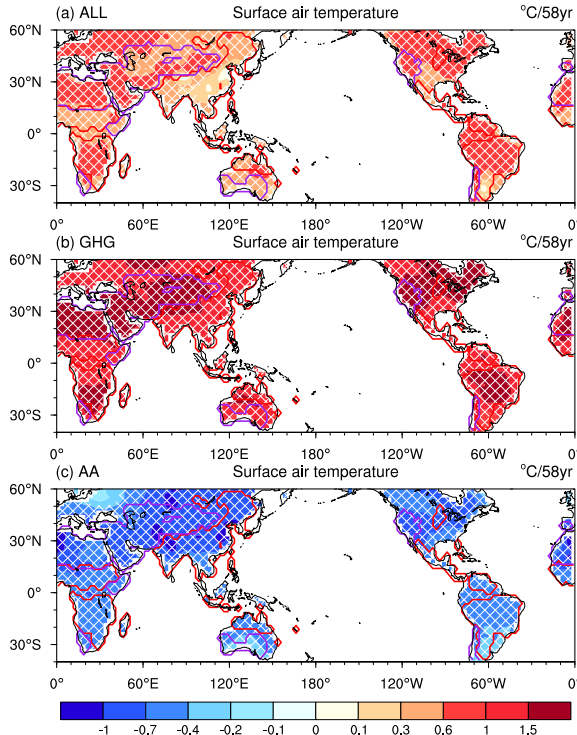
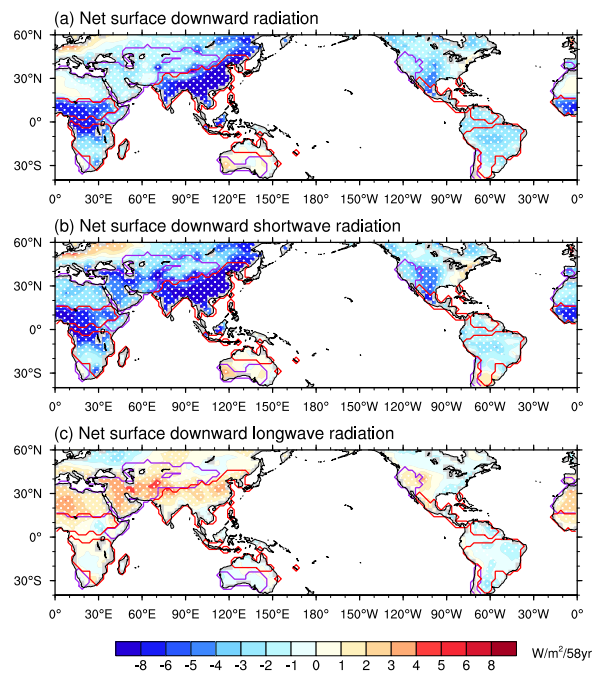


Figure 9. The trends of the precipitable water during the local summer of 1948–2005 for the multi-model ensemble mean of (a) ALL-forcing, (b) GHG-forcing and (c) AA-forcing simulations. The stippling indicates a 10% significance level. The red lines denote the global monsoon regions.

How did the aerosol and GHG changes affect the regional features of monsoon precipitation? For the thermodynamic component of vertical moisture advection, which reduces under the aerosol forcing due to that in specific humidity as the surface cools down, is significant over all land monsoon regions (Fig. 8c and e). In contrast, the GHG forcing increases the specific humidity and hence the thermodynamic component of moisture advection, which is also significant over all land monsoon regions (Fig. 8g and i). The examination of column integrated precipitable water changes shows that the decline in AA-forcing has been offset by an increase in GHG-forcing (Fig. 9). Thus, the thermodynamic effect of GHGs is on par with but opposes the effects of aerosols on precipitation.



411
412 **Figure 10.** The trends of the surface air temperature during the local summer of 1948~2005 for
413 the multi-model ensemble mean of (a) ALL-forcing, (b) GHG-forcing and (c) AA-forcing
414 simulations. The stippling indicates a 10% significance level. The red lines denote the global
415 monsoon regions.



416
417 **Figure 11.** The trends of the (a) net surface downward radiation, (b) net surface downward
418 shortwave radiation, and (c) net surface downward longwave radiation during the local summer of

419 1948~2005, for the multi-model ensemble mean of the AA-forcing simulations. The stippling
420 indicates a 10% significance level. The red lines denote the global monsoon regions.

421
422 Both the GHG-forcing and AA-forcing experiments show a reduction in the dynamic
423 component of moisture advection in the context of globally averaged precipitation over land
424 monsoon regions (Fig. 8a). While the reduction in GHG-forcing is understood to result from
425 increased atmospheric stability and, hence, weakened tropical circulation under global warming
426 (Held et al., 2006; Schneider et al., 2010; Chou et al., 2013b; Lau and Kim, 2017; Pascale et al.,
427 2017), the reduction in AA-forcing results from weakening of the monsoon circulation as a result
428 of the weakened land-ocean thermal contrast and hemispheric asymmetry (i.e., the northern
429 hemisphere is colder than the southern hemisphere (Lau and Kim., 2017)). This is caused by
430 aerosol-induced reductions in downward shortwave radiation through aerosol-radiation and
431 aerosol-cloud interactions (Figs. 10 and 11).

432 Distinctive regional patterns should be noticed. While the reduction in the dynamic term of the
433 GHG forcing simulation is evident and significant over nearly all land monsoon regions, no well-
434 organized consistent change pattern is seen in the AA-forcing simulation; the reduction is weak
435 and only significant over the Asian monsoon region and parts of the North and South American
436 monsoon regions, while parts of the African monsoon region even witness an increase in
437 precipitation. The dynamic response of regional monsoon circulation to aerosol forcing deserves
438 further study.

439 **4 Conclusions and discussions**

440 In this study, we find that anthropogenic forcing has had a detectable and attributable influence
441 on the significant drying trend of the global land monsoon precipitation during 1948~2005. The
442 optimal fingerprinting analysis shows that the observed drying trend ($-10.55 \text{ mm month}^{-1} (58 \text{ yr})^{-1}$)
443 is attributable to anthropogenic aerosols, with a contribution of 102% (62~144% for the 5~95%
444 confidence interval). A moisture budget analysis reveals that the drying trend in monsoon
445 precipitation results from the reduction in vertical moisture advection due to aerosol forcing. The
446 cooling effects of aerosol forcing are two-fold: a thermodynamic effect due to the reduction in
447 atmospheric humidity and a dynamic effect due to weakening of the land-sea thermal contrast and
448 thus monsoon circulation. Both contribute to the reduction in vertical moisture advection. The
449 warming effects of GHG forcing are also two-fold: a thermodynamic effect, which increases
450 atmospheric moisture, and a dynamic effect, which reduces vertical advection by increasing
451 atmospheric stability. The thermodynamic and dynamic effects largely offset each other, resulting
452 in a weak net wetting trend.

453 Our demonstration on the effects of anthropogenic aerosol on the drying trend in global
454 monsoon precipitation has important implications for the future. Since much of the monsoon
455 regions, such as India, are also regions of rapid development with increasing aerosol emissions (Li
456 et al., 2016), our results imply that there would be a further reduction in monsoon precipitation in
457 these regions if a clean energy policy is not deployed for effective mitigation in the future. Since
458 the late 1970s, the sulphate aerosol emissions in China has gradually increased, with a decline after
459 2006 because of adjustment of energy structure in China (Li et al., 2017). The reduction in aerosols
460 emissions not only improved the air quality, but also the water resources in monsoon regions.
461 Given the availability of the monsoon simulation, this study only focused on 1948~2005. Previous
462 studies have shown that the global monsoon precipitation has experienced a recovery since 1979
463 (Wang et al., 2012; Lin et al., 2014). There is lack of detection and attribution studies to quantify
464 the relative contributions of different external forcings to this increasing trend, although studies

465 indicated that the anthropogenic greenhouse gases may play a role (Wang et al., 2012; Zhang and
466 Zhou, 2014).

467 Although we used ensemble simulations from CMIP5, particularly multi-model and members,
468 to increase the robustness of the results, we note that there are still large uncertainties in the
469 estimation of aerosol forcing on precipitation changes due to the complexity of aerosol climate
470 effects, including the direct and indirect effects of aerosols (Wu et al., 2018; Li et al., 2016; Zhou
471 et al., 2018). Limited observational and cloud-resolving modeling studies suggest that the net
472 effect (enhance or suppress) of aerosol on precipitation relies on the aerosol type, meteorological
473 background (such as cloud-water content), precipitation intensity, region of interest, etc. (Zhao et
474 al., 2006; Qian et al., 2009; Li et al., 2011). The aerosol satellite observations and stational
475 precipitation observations show that the increase in aerosol concentration in China during the past
476 several decades can increase the atmospheric stability, weaken vertical motion and reduce total
477 rainfall over eastern China (Zhao et al., 2006). Aerosols can also increase cloud droplet number
478 concentration, reduce the cloud droplet size and thus contribute to the decreasing trend in light
479 rainfall over eastern China (Qian et al., 2009). In addition, the quality of aerosol forcing in each
480 monsoon region used to force the historical simulations exists large uncertainty. There is
481 substantial uncertainty in present-day top-of-atmosphere aerosol effective radiative forcing, with
482 a 5%-to-95% confidence interval spanning -1.9 W m^{-2} to -0.1 W m^{-2} (Myhre et al., 2013). The
483 uncertainty in aerosol radiative forcing is one of the uncertainty sources for detection and
484 attribution results and the associated physical understanding. The undergoing sixth phase of
485 Coupled Model Intercomparison Project (CMIP6, Eyring et al., 2016) updated the historical
486 anthropogenic aerosol forcing, greenhouse gas forcing and land use forcing, which are used for the
487 Detection and Attribution Model Intercomparison Project (DAMIP, Gillett et al., 2016). The new
488 output would provide solid data support for the attribution studies of monsoon precipitation
489 changes. It is desirable to examine the monsoon precipitation response to aerosol forcing based on
490 the newly released CMIP6 output. We should note that the multi-model framework of CMIP may
491 also include structural or parametric uncertainties. It remains a challenge in the climate research
492 community as to improve the model simulation of the aerosol-monsoon interaction, and to reduce
493 uncertainties in aerosol-climate feedback based on observations (Li et al., 2011; Wu et al., 2015;
494 Zhou et al., 2018).

497 Acknowledgments

498 This work is jointly supported by the CAS Strategic Priority Research Program (XDA20060102),
499 China MOST program (2018YFC1507701) and the National Natural Science Foundation of China
500 (Grant Nos. 41775091). Yun Qian's contribution is supported as part of the Energy Exascale Earth
501 System Model (E3SM) project, funded by the U.S. Department of Energy, Office of Science,
502 Office of Biological and Environmental Research. The Pacific Northwest National Laboratory
503 (PNNL) is operated for DOE by Battelle Memorial Institute under contract DE-AC06-76RLO
504 1830. We also acknowledge the support from Jiangsu Collaborative Innovation Center for Climate
505 Change. The CMIP5 simulations used in this paper can be accessed from <https://esgf-node.llnl.gov/search/cmip5/>. Observational precipitation datasets for GPCC, University of
506 Delaware, PREC/L, and GHCN are available from <https://www.esrl.noaa.gov/psd/data/>, while for
507 CRU is from <https://crudata.uea.ac.uk/cru/data/precip/>, and for VASClmO is from
508 <http://iridl.ldeo.columbia.edu/SOURCES/.DEKLIM/.VASClmO/.PrcpClim/#info>.
509

511 **References**

512 Allen M and Tett S. 1999. Checking for model consistency in optimal fingerprinting. *Clim Dynam*,
513 15(6): 419–434.

514 Allen M and Stott P 2003. Estimating signal amplitudes in optimal fingerprinting, Part I: Theory.
515 *Clim Dynam*, 21(5-6), 477–491.

516 Annamalai H, Hafner J, Sooraj K, Pillai P. 2013 Global warming shifts the monsoon circulation,
517 drying South Asia. *J Clim*, 26: 2701–2718. <https://doi.org/10.1175/JCLI-D-12-00208.1>

518 Beck C, Grieser J and Rudolf B. 2005. A new monthly precipitation climatology for the global
519 land areas for the period 1951 to 2000. DWD, *Klimastatusbericht KSB* 2004, ISSN 1437-
520 7691, ISSN 1616-5063 (Internet), ISBN 3-88148-402-7, 181–190.

521 Bindoff N, Stott P, AchutaRao K, Allen M, Gillett N, Gutzler D, Hansingo K, Hegerl G, Hu Y, Jain
522 S, Mokhov I, Overland J, Perlitz J, Sebbari R and Zhang X, 2013. Detection and
523 attribution of climate change: from global to regional. In: *Climate Change 2013: The
524 Physical Science Basis. Contribution of Working Group I to the Fifth Assessment Report
525 of the Intergovernmental Panel on Climate Change*. Stocker, T.F., D. Qin, G.-K. Plattner,
526 M. Tignor, S.K. Allen, J. Boschung, A. Nauels, Y. Xia, V. Bex and P.M. Midgley eds..
527 Cambridge : Cambridge University Press. 86.

528 Bollasina M, Ming Y and Ramaswamy V. 2011. Anthropogenic aerosols and the weakening of the
529 South Asian summer monsoon. *Science*, 334(6055): 502–505.

530 Chen M, Xie P, Janowiak J, and Phillip A. 2002. Global land precipitation: A 50-yr monthly
531 analysis based on gauge observations. *J. Hydrometeorol.* 3(3): 249–266.

532 Chen X and Zhou T. 2015. Distinct effects of global mean warming and regional sea surface
533 warming pattern on projected uncertainty in the South Asian summer monsoon. *Geophys
534 Res Lett*, 42(21): 9433–9439.

535 Chou C, Wu T and Tan P. 2013a. Changes in gross moist stability in the tropics under global
536 warming. *Clim Dynam*, 41(9-10):2481–2496.

537 Chou C, Chiang J, Lan C, Chung C, Liao Y, Lee C. 2013b. Increase in the range between wet and
538 dry season precipitation. *Nat Geosci*, 6(4): 263–267.

539 Dong B, Sutton R, Highwood E, Wilcox L. 2016. Preferred response of the East Asian summer
540 monsoon to local and non-local anthropogenic sulphur dioxide emissions. *Clim Dyn*,
541 46:1733–1751. doi:10.1007/s00382-015-2671-5.

542 Eyring V, Bony S, Meehl G A, Senior C A, Stevens B, Stouffer R J, and Taylor K E. 2016.
543 Overview of the Coupled Model Intercomparison Project Phase 6 (CMIP6) experimental
544 design and organization, *Geosci Model Dev*, 9: 1937–1958, doi:10.5194/gmd-9-1937-2016.

545 Gillett N, Shiogama H, Funke B, Hegerl G, Knutti R, Mattes K, Santer B, Stone D, Tebaldi C.
546 2016. The Detection and Attribution Model Intercomparison Project (DAMIP v1.0)
547 contribution to CMIP6. *Geoscientific Model Development*, 9:3685–3697.

548 Guo L, Highwood E, Shaffrey L and Turner A. 2013. The effect of regional changes in
549 anthropogenic aerosols on rainfall of the East Asian Summer Monsoon. *Atmospheric Chem
550 Phys.* 13(3):1521–1534.

551 Harris I, Jones P, Osborn T and Lister D. 2014. Updated high-resolution grids of monthly climatic
552 observations – the CRU TS3.10 Dataset. *Int J Climatol*, 34(3): 623–642.

553 Held I, Delworth T, Lu J, Findell K. and Knutson T. 2005. Simulation of Sahel drought in the 20th
554 and 21st centuries. *Proc. Natl Acad. Sci.* 102(50): 17891–17896.

555 Held I and Soden B. 2006. Robust responses of the hydrological cycle to global warming. *J Clim*,

556 19(21): 5686–5699.

557 Hegerl G, Hoegh-Guldberg O, Casassa G, Hoerling M, Kvats S, Parmesan C, Pierce D, Stott P.

558 2010. Good practice guidance paper on detection and attribution related to anthropogenic

559 climate change. In: Meeting Report of the Intergovernmental Panel on Climate Change

560 Expert Meeting on Detection and Attribution of Anthropogenic Climate Change. T. F.

561 Stocker, et al. eds.. IPCC Working Group I Technical Support Unit, University of Bern,

562 Bern, Switzerland, 8.

563 Huang X, Zhou T, Turner A, Dai A, Chen X, Clark R, Jiang J, Man W, Murphy J, Rostro J, Wu

564 B, Zhang L, Zhang W, Zou L. 2020. The Recent decline and recovery of Indian summer

565 monsoon rainfall: relative roles of external forcing and internal variability. *J Clim*,

566 <https://doi.org/10.1175/JCLI-D-19-0833.1>

567 Jiang J, Zhou T. 2019. Global monsoon responses to decadal sea surface temperature variations

568 during the twentieth century: Evidence from AGCM simulations. *J Clim*, 32: 7675–7695.

569 doi: 10.1175/JCLI-D-18-0890.1

570 Jiang Y, Liu X, Yang X Q, Wang M. 2013. A numerical study of the effect of different aerosol

571 types on East Asian summer clouds and precipitation, *Atmospheric Environment*, 70:

572 51–63, doi: 10.1016/j.atmosenv.2012.12.039.

573 Jiang Y, Yang X Q, and Liu X. 2015. Seasonality in anthropogenic aerosol effects on East Asian

574 climate simulated with CAM5, *Journal of Geophysical Research – Atmospheres*, 120:

575 10837–10861, doi: 10.1002/2015JD023451

576 Kitoh A, Endo H, Kumar K, Cavalcanti I, Goswami P, Zhou T. 2013. Monsoons in a changing

577 world: a regional perspective in a global context. *J Geophys Res*, 118(8): 3053–3065.

578 Krishnan R, Sabin T, Vellore R, Mujumdar M, Sanjay J, Goswami B, Hourdin F, Dufresne J, Terray

579 P. 2016. Deciphering the desiccation trend of the South Asian monsoon hydroclimate in a

580 warming world. *Climate Dynamics*, 47 (3):1007–1027.

581 Krushnamurthy L and Krishnamurthy V. 2014. Influence of PDO on South Asian summer monsoon

582 and monsoon–ENSO relation. *Climate Dynamics*, 42: 2397–2410.

583 Lamarque J, Bond T, Eyring V, Granier C, Heil A, Klimont Z, Lee D, Liousse C, Mieville A, Owen

584 B, Schultz M, Shindell D, Smith S, Stehfest E, J. Van Aardenne, Cooper O, Kainuma M,

585 Mahowald N, McConnell J, Naik V, Riahi K, and van Vuuren D. 2010. Historical (1850–

586 2000) gridded anthropogenic and biomass burning emissions of reactive gases and aerosols:

587 Methodology and application, *Atmos Chem Phys*, 10: 7017–7039.

588 Lau K, Kim M and Kim K. 2006. Asian summer monsoon anomalies induced by aerosol direct

589 forcing: the role of the Tibetan Plateau. *Clim Dynam*, 26(7-8): 855–864.

590 Lau W and Kim K. 2017. Competing influences of greenhouse warming and aerosols on Asian

591 summer monsoon circulation and rainfall. *Asia-Pac J Atmospheric Sci*, 53(2): 181–194.

592 Li H, Dai A, Zhou T. and Lu J. 2010. Responses of East Asian summer monsoon to historical SST

593 and atmospheric forcing during 1950–2000. *Clim Dynam*, 34(4): 501–514.

594 Li M, Liu H, Geng G, Hong H, Liu F, Song Y, Tong D, Zheng B, Cui H, Man H, Zhang Q, He K.

595 2017. Anthropogenic emission inventories in China: a review. *National Science Review*, 4:

596 834–866, 2017, doi: 10.1093/nsr/nwx150

597 Li Z, Lau W, Ramanathan V, Wu G, Ding Y, Manoj M, Liu J, Qian Y, Li J, Zhou T, Fan J, Rosenfeld

598 D, Ming Y, Wang Y, Huang J, Wang B, Xu X, Lee S, Cribb M, Zhang F, Yang X, Zhao C,

599 Takemura T, Wang K, Xia X, Yin Y, Zhang J, Guo J, Zhai P, Sugimoto N, Babu S, Brasseur

600 G. 2016. Aerosol and monsoon climate interactions over Asia. *Rev Geophys*, 54 (4):

601 866–929.

602 Li Z, Li C, Chen H, Tsay S, Holben B, Huang J, Li B, Maring H, Qian Y, Shi G, Xia X, Yin Y,
603 Zheng Y, Zhuang G. 2011. East Asian studies of tropospheric aerosols and their impact on
604 regional climate (EASTAIRC): an overview, *J Geophys Res*, 116, D00K34,
605 doi:10.1029/2010JD015257.

606 Lin R, Zhou T, Qian Y. 2014. Evaluation of global monsoon precipitation changes based on five
607 reanalysis datasets, *J Clim*, 27(3): 1271–1289, doi: <http://dx.doi.org/10.1175/JCLI-D-13-00215.1>

609 Meehl G, Arblaster J and Collins W. 2008. Effects of black carbon aerosols on the Indian monsoon.
610 *J Clim*, 21(12): 2869–2882.

611 Ma S, Zhou T, Stone D, Polson D, Dai A, Stott P, Storch H, Qian Y, Burke C, Wu P, Zou L, and
612 Ciavarella A. 2017. Detectable anthropogenic shift toward heavy precipitation over eastern
613 China. *J Clim*, 30: 1381–1396, doi:10.1175/JCLI-D-16-0311.1.

614 Myhre G, Shindell D, Bréon F M, Collins W, Fuglestvedt J, Huang J, et al. 2013. Anthropogenic
615 and natural radiative forcing – in *Climate Change 2013: the Physical Science Basis*.
616 Contribution of Working Group I to the Fifth Assessment Report of the Intergovernmental
617 Panel on Climate Change. Cambridge University Press,
618 <https://doi.org/10.1017/CBO9781107415324>

619 Pascale S, Boos W, Bordoni S, Bordoni S, Delworth T, Kapnick S, Murakami H, Vecchi G, Zhang
620 W. 2017. Weakening of the North American monsoon with global warming. *Nat Clim
621 Change*, 7(11): 806.

622 Paul S, Ghosh S, Oglesby R, Pathak A, Chandrasekharan A, Ramsankaran R. 2016 Weakening of
623 Indian summer monsoon rainfall due to changes in land use land cover. *Sci Rep*, 6:32177.

624 Peterson T and Vose R. 1997. An overview of the Global Historical Climatology Network
625 temperature database. *Bull Am Meteorol Soc*, 78(12): 2837–2849.

626 Polson D, Bollasina M, Hegerl G and Wilcox L. 2014. Decreased monsoon precipitation in the
627 Northern Hemisphere due to anthropogenic aerosols. *Geophys Res Lett*, 41(16): 6023–
628 6029.

629 Rotstayn L, Jeffrey S, Collier M, Dravitzki S, Hirst A, Syktus J and Wong K. 2012. Aerosol- and
630 greenhouse gas-induced changes in summer rainfall and circulation in the Australasian
631 region: a study using single-forcing climate simulations, *Atmos Chem Phys*, 12:
632 6377–6404.

633 Salzmann M, Weser H, Cherian R. 2014. Robust response of Asian summer monsoon to
634 anthropogenic aerosols in CMIP5 models. *Journal of Geophysical Research: Atmospheres*,
635 119 (19):11321–311337.

636 Qian Y, Flanner M, Leung L & Wang W. 2011. Sensitivity studies on the impacts of Tibetan Plateau
637 snowpack pollution on the Asian hydrological cycle and monsoon climate. *Atmospheric
638 Chem Phys*, 11(5): 1929–1948.

639 Qian Y, Gong D Y, Fan J W, Leung L R, Bennartz R, Chen D L, Wang W G. 2009. Heavy pollution
640 suppresses light rain in China: Observations and modeling. *J Geophys Res*, 114: D00K02,
641 doi: 10.1029/2008JD011575

642 Sato M, Hansen J, McCormick M, and Pollack J. 1993. Stratospheric aerosol optical depths, *J
643 Geophys Res*, 98: 22987–22994.

644 Schneider T, O'Gorman P and Levine X. 2010. Water vapor and the dynamics of climate changes.
645 *Rev Geophys*, 48, RG3001, <https://doi.org/10.1029/2009RG000302>.

646 Schneider U, Becker A, Finger P, Meyer-Christoffer A, Ziese M, and Rudo B. 2014. GPCC's new
647 land surface precipitation climatology based on quality-controlled in situ data and its role

648 in quantifying the global water cycle. *Theor Appl Climatol*, 115(1-2): 15–40.

649 Song F, Zhou T and Qian Y. 2014. Responses of East Asian summer monsoon to natural and
650 anthropogenic forcings in the 17 latest CMIP5 models. *Geophys Res Lett*, 41(2): 596–603.

651 Sun Y, Zhang X, Zwiers F, Song L, Wan H, Hu T, Yin H, Ren G. 2014. Rapid increase in the risk
652 of extreme summer heat in Eastern China. *Nature Climate Change*, 4(12): 1082.

653 Sun Y, Yin H, Tian Q, Hu T, Shi Y, Liu H, Zhou B. 2013. Recent progress in studies of climate
654 change detection and attribution in the globe and China in the Past 50 years. *Climate
655 Change Research* (in Chinese), 9(4): 235–245.

656 Taylor K E, Stouffer R J and Meehl G A. 2012. An overview of CMIP5 and the experiment design.
657 *Bull Am Meteorol Soc*, 93: 485–498.

658 Wang B, Ding Q. 2006. Changes in global monsoon precipitation over the past 56 years. *Geophys
659 Res Lett*, 33: L06711. doi:10.1029/2005GL025347

660 Wang B, Ding Q. 2008. Global monsoon: Dominant mode of annual variation in the tropics.
661 *Dynamics of Atmospheres and Oceans*, 44(3-4): 165–183.

662 Wang B, Liu J, Kim H, Webster P and Yim S. 2012. Recent change of the global monsoon
663 precipitation (1979–2008). *Clim Dynam*, 39(5): 1123–1135.

664 Wang B, Liu J, Kim HJ, Webster PJ, Yim SY, Xiang B. 2013. Northern Hemisphere summer
665 monsoon intensified by mega-El Nino/southern oscillation and Atlantic multidecadal
666 oscillation. *Proc Natl Acad Sci*, 110 (14):5347–5352.

667 Wang Z, Lin L, Yang M, Xu Y, Li J. 2017. Disentangling fast and slow responses of the East Asian
668 summer monsoon to reflecting and absorbing aerosol forcings. *Atmos Chem Phys*, 17 (18):
669 11075–11088, doi:10.5194/acp-17-11075-2017.

670 Willmott C, Matsuura K. 2001. Terrestrial air temperature and precipitation: Monthly and annual
671 time series (1950-1996). http://climate.geog.udel.edu/~climate/html_pages/README.ghcn_ts.html.

672 Wu G, Li Z, Fu C, Zhang X, Zhang R Y, Zhang R H, Zhou T, Li J, Li J, Zhou D, Wu L, Zhou L,
673 He B & Huang R. 2015. Advances in studying interactions between aerosols and monsoon
674 in China. *Sci China Earth Sci* (in Chinese), 45: 1–19. doi:10.1007/s11430-015-5198-z

675 Wu P, Christidis N, and Stott P. 2013. Anthropogenic impact on Earth's hydrological cycle. *Nat
676 Clim Change*, 3(9): 807–810.

677 Xu Y, Gao X, Shi Y, Zhou B. 2015. Detection and attribution analysis of annual mean temperature
678 changes in China. *Climate Research*, 63(1): 61–71.

679 Yang X, Zhu Y, Xie Q, Ren X, and Xu G. 2004. Advances in studies of Pacific Decadal Oscillation.
680 Chinese Journal of Atmospheric Sciences (in Chinese), 28(6): 979–992.

681 Zhang L and Zhou T. 2011. An assessment of monsoon precipitation changes during 1901–2001.
682 *Clim Dynam*, 37(1-2): 279–296.

683 Zhang L and Zhou T. 2014. An Assessment of Improvements in Global Monsoon Precipitation
684 Simulation in FGOALS-s2?, *Advances in Atmospheric Sciences*, 31(1): 165–178, doi:
685 10.1007/s00376-013-2164-6.

686 Zhang W, Zhou T, Zou L, Zhang L, and Chen X. 2018. Reduced exposure to extreme precipitation
687 from 0.5C less warming in global land monsoon regions. *Nature Communications*. 9: 3153.
688 doi:10.1038/s41467-018-05633-3

689 Zhang X, Zwiers F W, Hegerl G. C., et al. 2007. Detection of human influence on twentieth-century
690 precipitation trends. *Nature*, 448(7152): 461.

691 Zhao C, Tie X, and Lin Y. 2006. A possible positive feedback of reduction of precipitation and
692 increase in aerosols over eastern central China, *Geophys Res Lett*, 33, L11814,
693

doi:10.1029/2006GL025959.

Zhou T, Zhang L and Li H. 2008a. Changes in global land monsoon area and total rainfall accumulation over the last half century. *Geophys Res Lett*, 35(16).

Zhou T, Yu R, Li H, Wang B. 2008b. Ocean forcing to changes in global monsoon precipitation over the recent half-century. *J Clim*, 21(15): 3833–3852.

Zhou T, Wu B, Guo Z, He C, Zou L, Chen X, Zhang L, Man W, Li P, Li D, Yao J, Huang X, Zhang W, Zuo M, Lu J, Sun N. 2018. A review of East Asian summer monsoon simulation and projection: Achievements and problems, opportunities and challenges. *Chinese Journal of Atmospheric Sciences* (in Chinese), 42 (4): 902–934, doi:10.3878/j.issn.1006-9895.1802.17306.

Zhu Y, Yang X. 2003. Relationships between Pacific Decadal Oscillation and climate variabilities in China. *Acta Meteorologica Sinica* (in Chinese), 61(6):641–654.